Nano Today 53 (2023) 102024

Contents lists available at ScienceDirect

Nano Today

journal homepage: www.elsevier.com/locate/nanotoday

N-heterocyclic carbenes – The design concept for densely packed and thermally ultra-stable aromatic self-assembled monolayers

Mateusz Wróbel [a], Daria M. Cegiełka [a,b], Andika Asyuda [c], Krzysztof Kozieł [d], Michael Zharnikov [c,*], Piotr Cyganik [a,*]

[a] Jagiellonian University, Faculty of Physics, Astronomy and Applied Computer Science, Smoluchowski Institute of Physics, Łojasiewicza 11, 30-348 Krakow, Poland
[b] Jagiellonian University, Doctoral School of Exact and Natural Sciences, Łojasiewicza 11, 30-348 Krakow, Poland
[c] Angewandte Physikalische Chemie, Universität Heidelberg, Im Neuenheimer Feld 253, D-69120 Heidelberg, Germany
[d] Faculty of Chemistry, Jagiellonian University, Gronostajowa 2, 30-387 Krakow, Poland

ARTICLE INFO

Keywords:
N-heterocyclic carbenes
Self-assembled monolayers
Thermal stability
Packing density
NEXAFS
SIMS

ABSTRACT

Self-assembled monolayers (SAMs) of N-heterocyclic carbenes (NHCs) on metal substrates are currently one of the most promising systems in context of molecular-scale engineering of surfaces and interfaces, crucial for numerous applications. Interest in NHC SAMs is mainly driven by their assumingly higher thermal stability compared to thiolate SAMs most broadly used at the moment. Most of the NHC SAMs utilize imidazolium as an anchoring group for linking molecules to the metal substrate via carbene C atom. It is well established in the literature that standing up and stable NHC SAMs are built only when using bulky side groups attached to nitrogen heteroatoms in imidazolium moiety, which, however, leads to monolayers exhibiting much lower packing density compared to thiolate SAMs. Here, by combined X-ray photoelectron spectroscopy, near-edge X-ray absorption fine structure spectroscopy, and temperature-programmed secondary ion mass spectrometry analysis, we demonstrate that using NHCs with small methyl side groups in combination with simple, solution-based preparation leads to the formation of aromatic monolayers exhibiting at least doubled surface density, upright molecular orientation, and ultra-high thermal stability compared to the NHC SAMs reported before. These parameters are crucial for most applications, including, in particular, molecular and organic electronics, where aromatic SAMs serve either as a passive element for electrode engineering or as an active part of organic field effect transistors and novel molecular electronics devices.

Introduction

Self-assembled monolayers (SAMs) [1,2] provide a versatile tool for engineering of surfaces and interfaces and are commonly used for numerous applications in biotechnology [3,4], molecular/organic electronics [5,6], and many other areas of modern science and technology. The key requirements in this context are (i) dense molecular packing, (ii) upright molecular orientation, and (iii) high thermal and chemical stability. Currently, most of SAM applications involving metal substrates rely on using thiolates (Fig. 1a) [1,2,7], however, an alternative direction was proposed [8–11] which exploits N-heterocyclic carbenes (NHCs). This development is based mainly on experimental [10–12] and theoretical [13,14] studies indicating significantly higher thermal and chemical stability of NHC SAMs compared to thiolates [15]. With few exceptions [16–18], NHC SAMs reported so far are formed using imidazolium moiety which links NHC molecules with the metal substrate (Au, Cu, Ag, Pt and Pd) through carbene C atom (Fig. 1b-d) [19–25]. The experimental data [22–28] and density functional theory (DFT) calculations [14,23,26,27,29] indicate that the molecular orientation in the NHC SAMs - either upright (Fig. 1b) or planar (Fig. 1c) toward the substrate - is predominantly determined by the size of side groups attached to nitrogen heteroatoms in this moiety, such as methyl (Me), ethyl (Et) or isopropyl (iPr). The packing density and bonding configuration are impacted accordingly, which defines a range of possible applications of the NHC SAMs. With a very few exceptions [30,31], which were later questioned both by spectroscopic [22,27] and microscopic [23] analysis, it was concluded that upright-oriented and thermally stable monolayers on metal substrates are only formed by NHCs with bulky side groups (Fig. 1b), whereas short methyl substituents lead to flat-oriented metal complexes exhibiting very low

* Corresponding authors.
E-mail addresses: michael.zharnikov@urz.uni-heidelberg.de (M. Zharnikov), piotr.cyganik@uj.edu.pl (P. Cyganik).

https://doi.org/10.1016/j.nantod.2023.102024
Received 5 June 2023; Received in revised form 20 September 2023; Accepted 8 October 2023
Available online 14 October 2023

surface density (Fig. 1c). Such design concept [14,22,26–29,32], based on vacuum-deposited NHC monolayers and supported by DFT calculations, became in recent years the main strategy for NHC SAM formation, with BIM^{iPr} (which contains bulky isopropyl side groups - see Fig. 2) being the most widely analyzed NHC platform for functionalization of metal substrates [10,11,14,22,26,27,33] and nanoparticles [34,35]. The most recent microscopic analysis [26] of BIM^{iPr}/Au shows molecular footprint (~57.5 $Å^2$) which is almost 3 times larger than that for thiolate SAMs on the same substrate (~21.6 $Å^2$) [1]. Such a low packing density, associated with the bulky side groups, results in low density of functional tail groups at the SAM-ambient interface, noticeably diminishing the chemical and physical impact of the functionalization and hindering thus the potential of NHC SAMs for surface and interface engineering (Fig. 1b). Therefore, it is urgently needed to find a strategy for the formation of NHC SAMs having packing density and, consequently, a functionalization ability comparable to those of thiolates and unfolding, at the same time, the expected potential of NHCs in terms of thermal stability (Fig. 1d).

To address this fundamental problem, we analyze a series of three NHC SAMs on Au(111) (Fig. 2) based on imidazolium (IM) unit with short Me side groups and different number n of benzene moieties coupled to this unit in acene fashion: IM ($n = 0$), BIM ($n = 1$) and NIM ($n = 2$). In contrast to the vacuum deposition approach used in most of the previous studies, these SAMs were prepared by immersion procedure, which was one of the key points to achieve the results reported below. The fabricated SAMs with Me side groups are compared with a similarly prepared monolayer with bulky side groups, BIM^{iPr}/Au considering the most basic parameters, such as packing density, film thickness, molecular inclination, and thermal stability. Our study provides direct experimental evidence that, contrary to the commonly established design principles for NHC SAMs, the NHC molecules with short methyl side groups can form, via solution-based fabrication procedure, upright-oriented monolayers and thus provide, for the first time, packing density comparable to that of standard thiolate SAMs on Au. Moreover, we show that the combination of the short side group with attachment of phenyl or naphthalene moiety to the anchoring imidazolium unit drastically improves the thermal stability of NHC SAMs. As the result, the current analysis allows us to propose an alternative concept for the formation of functional NHC SAMs.

Materials and methods

Detailed description of the synthetic protocols and information on the materials and methods can be found in the Supplementary Information.

Syntheses

All NHCs were synthesized according to literature protocols.

Sample preparation

For XPS, NEXAFS spectroscopy, and contact angle measurements, silicon wafers covered with ~100 nm of gold served as substrates. For SIMS measurements, mica substrates with ~100 nm of gold were used, in view of the higher thermal stability of this substrate type compared to Au/Si. Note that both Au/Si and Au/mica substrates are most typical and frequently used polycrystalline gold supports for the fabrication and characterization of SAMs, exposing predominantly Au(111) surface and mimicking excellently Au(111) single crystals in regard to SAM properties and characteristics [1,2]. These supports are also directly relevant for applications, in which the respective deposition routes can be easily adapted. The samples were prepared by immersing substrates in 1 mM solutions of the SAM precursors for ~20 h. Degassed THF and absolute ethanol were used as solvents for NHCs and thiols (reference systems), respectively. Preparation of the samples was performed in argon-filled glovebox.

XPS measurements

Al Kα (E = 1486.6 eV) X-ray source and VG SCIENTA R3000 spectrometer were used for the XPS measurements. The binding energy scale was referenced to the Au $4f_{7/2}$ peak at 84.0 eV. The inelastic background was subtracted using the Shirley function. Additional XPS measurements were performed at the synchrotron; see SI for details.

NEXAFS measurements

The measurements were performed at the HE-SGM beamline of the synchrotron radiation facility BESSY II (Berlin, Germany). The spectra were acquired at carbon and nitrogen K-edges. X-ray incidence angle was varied to monitor the linear dichroism effects linked to orientation of the molecules in the monolayers.

SIMS measurements

TOF SIMS V system (IONTOF GmbH) equipped with a 30 keV Bi^+ ion source and a time-of-flight analyzer was used. During the TP-SIMS measurements, the temperature was linearly increased from room temperature to 750 K at a constant rate (β) of 3.75 K/min. The emission intensities were normalized to the room-temperature values before the analysis.

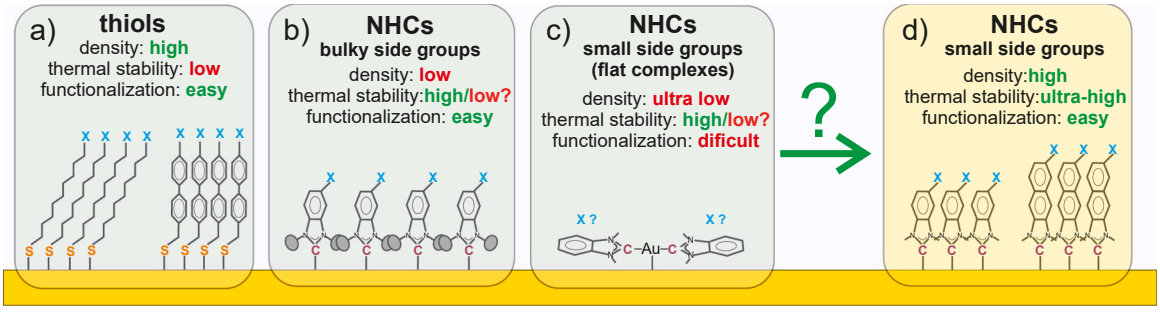

Fig. 1. Schematic comparison of structure, density, and thermal stability of thiolate and imidazolium-based NHC SAMs on Au. (a) High-density aliphatic/aromatic thiolate SAMs allow a versatile control of the SAM-ambient interface (by flexible selection of functional tail group, X) but have low thermal stability.[15] (b) Upright-oriented NHC SAMs with large side groups allow the same control of the SAM-ambient interface as thiolates but have much lower packing density and do not give any gain in thermal stability. (c) Flat-oriented NHC-Au-NHC complexes formed by NHC with small side groups have very low density, a problem with control of the SAM-ambient interface, and probably similar thermal stability as thiolates. (d) Optimized upright-oriented NHC SAMs with short side groups unite the advantages of all above systems and have high thermal stability in addition.

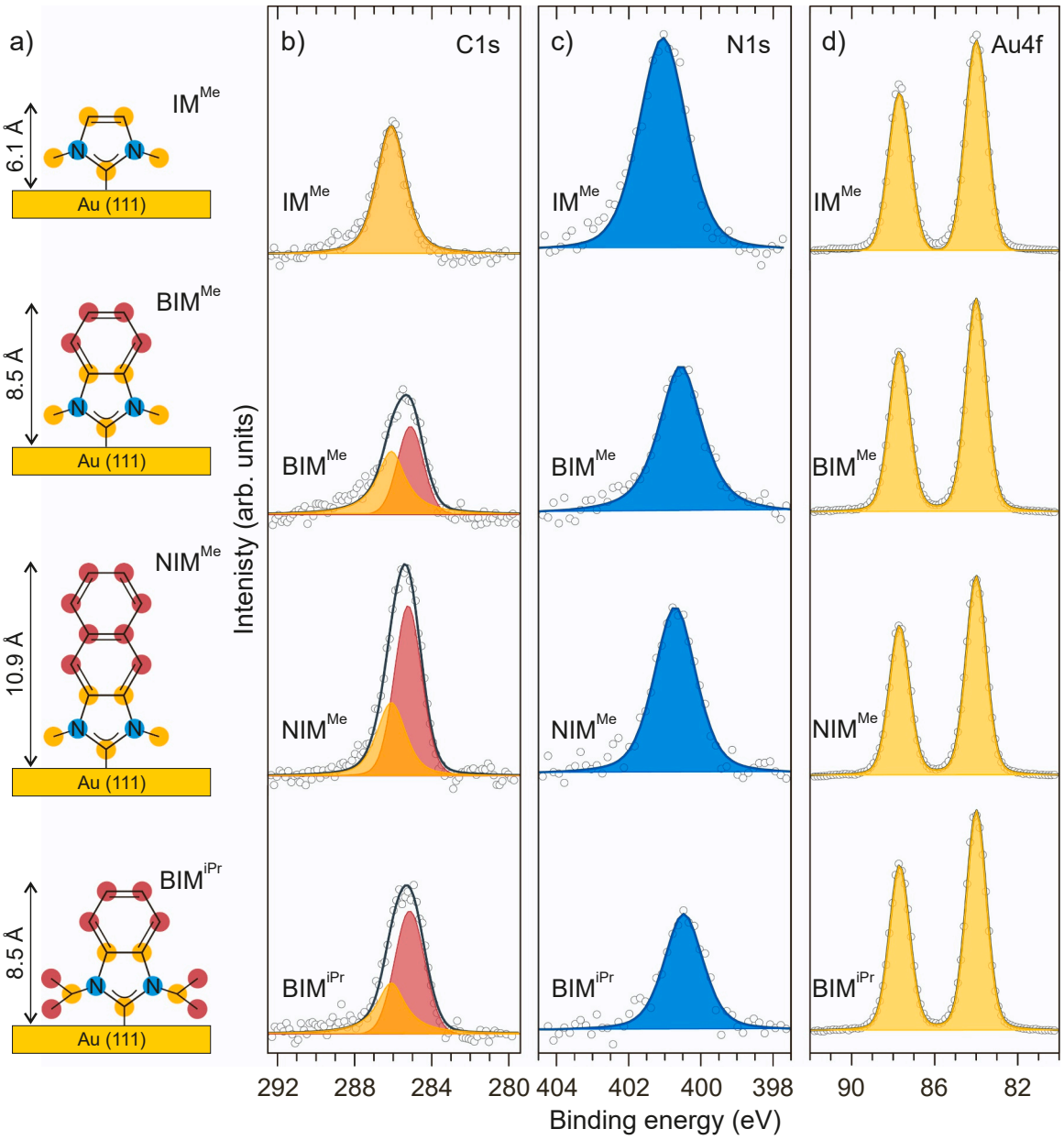

Fig. 2. XPS analysis. (a) Schematic drawings of the molecules used in this study (IM^{Me}, BIM^{Me}, NIM^{Me} and BIM^{iPr}) with indicated C atoms corresponding to IM unit (yellow), remaining aromatic or side groups (red), and N atoms (blue). The geometric heights of the molecules indicated in (a) were estimated assuming fully upright orientation and a length of the C-Au bond of ~2.1 Å.[11] (b-d) C 1s (b), N 1s (c), and Au 4f (d) spectra of the NHC SAMs. Individual components in the C 1s (red at ~285.0 eV and yellow at ~286.0 eV) and N 1s spectra (blue at ~401.0 eV for IM^{Me} or ~400.5 eV for BIM^{Me}, NIM^{Me} and BIM^{iPr}) are color-coded in relation to individual atoms in (a).

Surface energy analysis

For the calculation of the surface energies, measurements of the contact angles of water and diiodomethane were performed. The acquired data were statistically processed to obtain mean values and standard deviations that were used for the surface energy calculations using the Fowke's method.

Results and discussion

Spectroscopic analysis of the structure and bonding configuration

Successful adsorption of the NHC molecules on the substrate for all four SAMs is directly confirmed by the static secondary ion mass spectrometry (SIMS) which shows a strong emission of positive secondary ions corresponding to complete molecule (M^+) and molecule-metal clusters (MAu^+, M_2Au^+, $M_2Au_2^+$, MAu_3^+). The respective signal is generally considered as a "fingerprint" of SAMs with individual molecules chemically bound to a metal substrate (SI; Fig. S19) [36,37]. In contrast, for all these SAMs, the emission of corresponding negative molecular ions is negligible. Following former analysis [37] it is known in SIMS that the emission resulting from breaking of well-defined bond with an ionic character predominantly leads to ionization of the emitted fragments according to the partial charge in this bond, therefore, the preferable emission of M^+ in contrast to M^- indicates ionic character of the covalent molecule-metal bond (C-Au) for all analyzed NHC SAMs, with the positive charge accumulated at the carbene C atom. This conclusion is consistent with the DFT calculations [13,38,39] for NHC SAMs showing significant electron donation from the carbene carbon to gold substrate.

To analyse the thickness, density, and bonding configuration of the NHC SAMs, X-ray photoelectron spectra (XPS) in the C 1s, N 1s, and Au 4f ranges were taken (Fig. 2). The C 1s spectrum for the shortest member of the series, IM^{Me}/Au, exhibits a single symmetric peak at the binding energy (BE) of ~286.0 eV, in agreement with a former XPS study for this monolayer [23]. Interestingly, the terminal C atom of protonated (= chemically symmetric) imidazole has a higher (by ~1.2 eV) BE compared to two other C atoms in this moiety, so that the respective component in IM^{Me}/Au is shifted [40], as a consequence of bonding to the substrate and screening effects, resulting in only one peak for all three C atoms. In contrast, for the monolayers containing one (BIM^{Me}/Au and BIM^{iPr}/Au) or two (NIM^{Me}/Au) benzene moieties, this peak becomes asymmetric and two components are needed to fit the spectra properly. It is then logical to assume that the first component corresponds to the imidazolium unit, and the second is related to the carbon atoms in the benzene rings and more bulky side groups. Setting the intensity ratio of both components (on the basis of stoichiometry corrected by the respective attenuation factors; see SI for details) and fixing the position of the first component at ~286.0 eV, we obtained the position of the second component, which for BIM^{Me}/Au, NIM^{Me}/Au and BIM^{iPr}/Au turned out to be ~285.0 eV. Importantly, this position corresponds to a BE shift of ~0.9 eV in comparison to the BE typical of aromatic [41] or hybrid aromatic-aliphatic [42] thiolate/selenolate SAMs (~284.1 eV). This shift stems most likely from an electrostatic effect [43] caused by the charge rearrangement at the molecule-metal interface upon modification of the bonding group from thiols/selenols to carbene, and formation of the respective dipole layer. The direction of this shift is consistent with the charge transfer from the carbene carbon to the gold substrate, confirming the conclusion from the SIMS analysis.

The N 1s spectra of all NHC SAMs exhibit a single component, which suggests a chemical equivalence of both N atoms in imidazolium unit. This component is located at ~401.0 eV for IM^{Me}/Au but shifted to ~400.5 eV for the other NHC SAMs analysed here (Fig. 2). Note that all these values are higher than those known for amino group (~399–400 eV) [44]. Generally, the respective shift, which has the same direction as for the C 1s peak, could also be ascribed to dipole layer formation. However, the difference in its magnitude for IM^{Me}/Au and the other NHC SAMs indicates an increased interaction of nitrogen π-electron system with the metal substrate in the latter case [27] or, probably, a change in molecular organization and bonding configuration in the SAMs.

Note that apart from the major peaks described above, some of the C 1s and N 1s spectra in Fig. 2 contain weak shoulders at the high binding energy side of the main peaks. These shoulders are most likely related to residual contamination, trapped solvent molecules and, probably, a comparably small amount of physisorbed molecules that survived the post-preparation-washing. Such species are frequently found in different SAMs and do not affect their quality and parameters, as far as the respective contributions are small, which is the case here.

As a next step, the effective thickness of the monolayers was calculated on the basis of the C 1s/Au 4f intensity ratio (the total C 1s signal / the joint Au $4f_{7/2}$ and Au $4f_{5/2}$ signal) following well-established procedure [45] with previously reported attenuation lengths [46] and using hexadecanethiolate/Au as a reference system (see SI for details). The obtained thicknesses are compiled in Table 1 and, for all monolayers, are relatively close to the geometric molecular lengths shown in Fig. 2, suggesting that these are indeed monolayers comprised of upright-oriented molecules. Significantly, the effective thickness of BIM^{iPr}/Au (~9.0 Å) is the same as in the recently published [26] report for this system. At the same time, the thickness values for all SAMs studied differ distinctly from that for the flat-oriented NHC monolayers (~1.7 Å), reported in the same study [26]. Apart from this distinct difference, the exact thickness values in Table 1 should be taken with a grain of salt since the attenuation lengths of the photoelectrons used for our calculation refer to alkanethiolate monolayers and can be somewhat different for the NHC SAMs.

To estimate the packing density we calculated the relative molecular footprint (MF), i.e. the area per individual molecule in the NHC SAMs in comparison with the reference monolayer of azobenzene thiol (C_6H_5-N=N-C_6H_4-$(CH_2)_3$-SH, Azo-3) on Au(111) which was previously characterized by molecularly-resolved scanning tunneling microscopy (STM) [47]. The MF was determined assuming the proportionality of the N 1s signal to the packing density of the molecules on the surface and using the known packing density of the established Azo-3 system (24.6 $Å^2$) as the reference [47]. For all MF calculations, the attenuation of the N 1s signal by the given monolayer, including the specific geometry of the Azo-3 SAM in particular [45], was taken into the account (see the SI for details).

The obtained MFs are presented in Table 1 as both relative and absolute values and show that, within the given precision (~20%), the packing densities of IM^{Me}, BIM^{Me}, and NIM^{Me} on Au are similar to each other and close to that of the reference Azo-3 system. Apart from the absolute MF values for the Me-substituted SAMs, their similarity contradicts a possible planar geometry, which will impose a progressively increasing MF with the increasing length of the molecular backbone at going from IM^{Me} to BIM^{Me} and further to NIM^{Me}. For a rough approximation of such scenario, we can assume the structure reported for IM^{Me}-Au-IM^{Me} complexes [23] and simply rescale it for BIM^{Me} and NIM^{Me}, which gives us MFs of ~48.4, ~67.5 and ~86.5 $Å^2$ for IM^{Me}/Au, BIM^{Me}/Au, and NIM^{Me}/Au, respectively, in obvious contrast to the experimental data. The only way to resolve this contradiction is to assume an upright adsorption geometry in all these SAMs. This conclusion is additionally confirmed by the roughly doubled MF value (~46.0 $Å^2$) obtained by us for BIM^{iPr}/Au, which is not far away from the recently reported STM-derived value [26] (~57.5 $Å^2$) for this system.

The XPS provides yet another, and independent, indication that NHC-Au-NHC complexes are not formed in our case. It was shown previously [27] that formation of planar IM^{Me}-Au-IM^{Me} complexes is associated with an additional, higher (by ~1.1 eV) BE component of the Au 4f peaks, corresponding to Au adatoms in these complexes. Our high-resolution Au $4f_{7/2}$ XP spectra of IM^{Me}/Au do not exhibit this additional component as shown in Fig. S16.

In addition to the above analysis, the issue of molecular orientation in the NHC SAMs was addressed by NEXAFS spectroscopy, which was

Table 1
Overview of the parameters for the analyzed NHC SAMs.

Parameter	IM^{Me}	BIM^{Me}	NIM^{Me}	BIM^{iPr}
Effective thickness* (Å)	7.5(±0.4)	8.2(±0.4)	10.8(±0.5)	9.0(±0.5)
Average tilt angle (C K-edge) (°)	27.9(±3)	27.7(±3)	24.2(±3)	20.9(±3)
Average tilt angle (N K-edge) (°)	23.2(±4)	20.0(±4)	23.1(±4)	14.3(±4)
Mol. footprint (relative to Azo-3)**	0.94(±0.19)	1.19(±0.24)	1.12(±0.22)	1.85(±0.37)
Mol. footprint ($Å^2$)**	23.2(±4.6)	29.3(±5.9)	27.5(±5.5)	45.6(±9.1)
Desorption temperature (K)	461(±9)	621(±10)	623(±11)	454(±8)
Desorption energy (eV)	1.40(±0.02)	1.90(±0.03)	1.91(±0.03)	1.38(±0.02)
Surface energy (mJ/m^2)	54.7(±6.8)	48.4(±4.9)	47.7(±5.0)	47.7(±5.3)

*Errors were estimated as ~5% of the values.
**Errors were estimated as ~20% of the values.

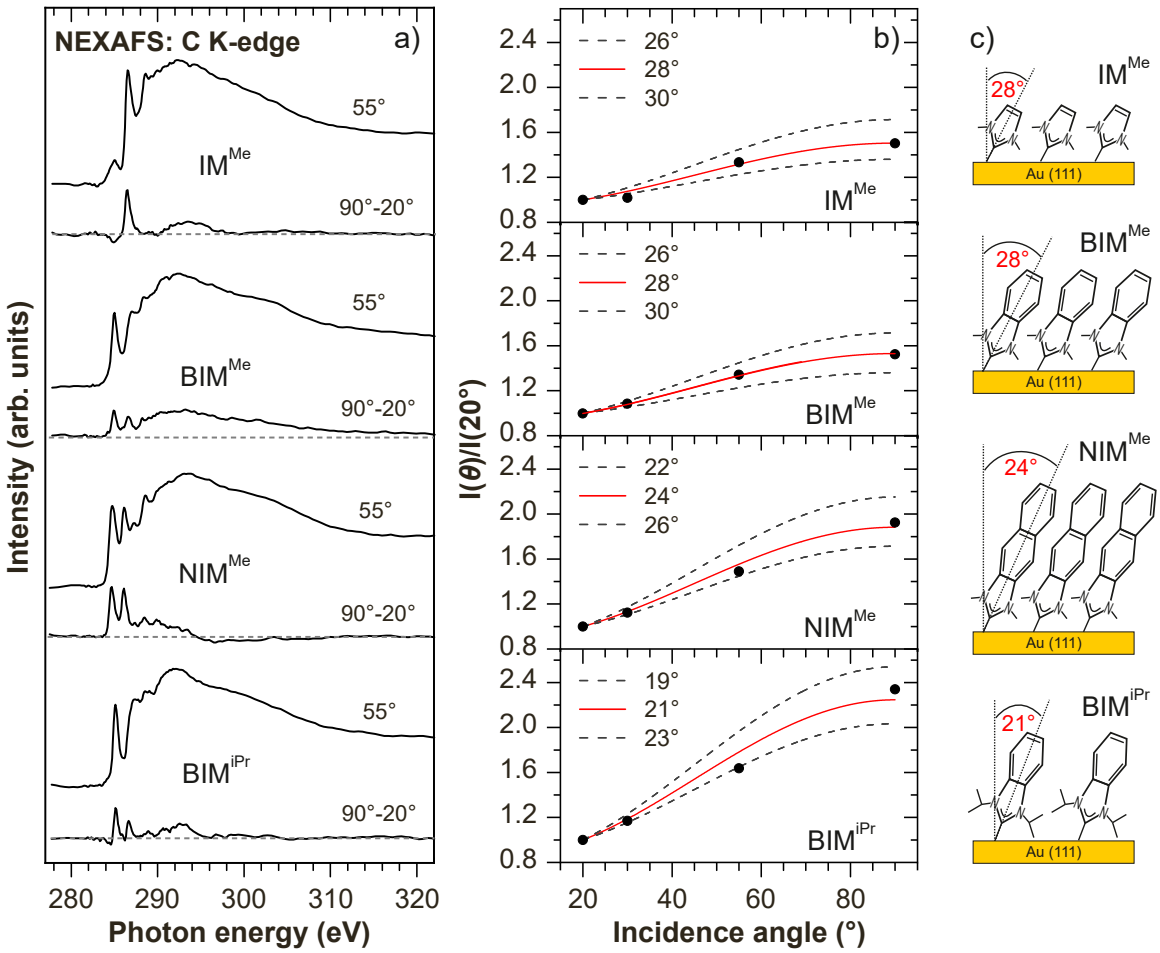

Fig. 3. NEXAFS analysis. (a) C K-edge NEXAFS spectra of the NHC SAMs measured at an X-ray incidence angle of 55° (to exclude orientational effects) along with the difference between the spectra acquired at the normal (90°) and grazing (20°) incidence (to monitor orientational effects). (b) The ratio of the π_1* resonance intensities as a function of the incidence angle (black circles). The best fits are shown by the red solid lines and the respective average tilt angles are given; the curves corresponding to slightly different tilt angles (±2°) are shown for comparison (black dashed lines). (c) Scheme of the molecular orientation in the NHC SAMs.

also useful to verify the chemical composition of the monolayers. The respective C K-edge data are summarized in Fig. 3, while complementary N K-edge data can be found in the SI.

The C K-edge spectrum of IM^{Me}/Au in Fig. 3a is dominated by the characteristic [48,49] π_1* resonance of imidazole at ~286.5 eV, accompanied by a weak π_2* resonance at ~288.6 eV and a variety of overlapping σ*-resonances. Note that the position of the π_1* resonance agrees perfectly with a recent NEXAFS study of the same system [27] and the spectrum of protonated imidazole.[47] The spectra of BIM^{Me}/Au and BIM^{iPr}/Au exhibit the characteristic π* signature of benzimidazole [50], i.e. a strong π_1* resonance at ~285.1 eV and a weaker π* resonance at ~286.7 eV, linked to the π_1* resonance of imidazole. Note that the positions of the π* resonances agree well with a recent NEXAFS study for a BIM-based SAM on Pt(111) [25]. The spectrum of NIM^{Me}/Au exhibits the characteristic π* signature of naphthalene [41], i.e. a double π* resonance at 284.65 eV and 286.1 eV. Thus, the chemical identity of the NHC SAMs is confirmed. Complementary information is provided by the N K-edge spectra (Fig. S17), which show only one π_1* resonance at 401.7 eV for IM^{Me}/Au, and two π* resonances at 401.7 eV and ~403 eV for BIM^{Me}/Au and NIM^{Me}/Au and somewhat lower energies for BIM^{iPr}/Au. Note that the resonance at 401.7 eV is generally observed in the spectra of NHC SAMs [24,25,27,28,51,52], accompanied sometimes by a further π* resonance at 399–399.7 eV [24,25,28,51,52], associated in some cases with a specific side-substitution and, alternatively, characteristic of a non-substituted N atom of imidazole [48,49]. The absence of the latter resonance and the presence of the resonance at 401.7 eV in our spectra suggest the expected chemical equivalence of both N atoms in imidazolium unit of the SAM-forming molecules, similar to the protonated form of imidazole [49]. The appearance of the additional π* resonance at ~403 eV in the BIM and NIM case is most likely a consequence of a coupling of the π* orbitals of the imidazolium moiety with the substrate, involving both or only one nitrogen atom being in closer proximity to the substrate because of possible molecular twist. Such a scenario seems to be supported by the recent DFT calculations of the projected density of states (PDOS) for the π* orbitals of nitrogen atoms of BIM^{Me} and BIM^{iPr} on Au(111) [53]. Accordingly, certain adsorption configurations of these molecules lead to appearance of two components of the π* orbital separated by c.a. 1.1–1.5 eV [53] which is quite close to 1.2–1.3 eV visible in our data. A more detailed discussion of the N K-edge data can be found in the SI.

Both C and N K-edge spectra exhibit pronounced linear dichroism, i.e. dependence of the intensity of the characteristic absorption resonances on the X-ray incidence angle, θ. As shown by the difference spectra in Fig. 3a and the spectra in Fig. S17, the intensity of the π* resonances at the normal X-ray incidence is higher than that at the grazing geometry. In view of the orientation of the E vector of the primary X-rays (*p*-polarization) and the orientation of the π* orbitals with respect to the molecular backbone (perpendicular to the aromatic rings), this relation suggests an upright molecular orientation in all NHC SAMs studied. The exact values of the average molecular tilt angles in these monolayers could be found by fitting the angular dependences of the π* resonance intensity by suitable theoretical curves for a vector-like

orbital with the tilt angle as fitting parameter (see SI for details). The respective curves are presented in Fig. 3b for the C K-edge data and in Fig. S18 for the N K-edge data. The derived average molecular tilt angles are marked in the figures and compiled in Table 1; in agreement with all other data, these values correspond to an upright molecular orientation in all SAMs studied, as also schematically illustrated in Fig. 3c. Note that the tilt angle values derived from the C and N K-edge data differ to some extent but correlate with each other within the given error bars. This difference is related to the limited accuracy of the measurements and the data evaluation procedure as well as to the low signal-to-noise ratio of the N K-edge spectra. Note also that it cannot be excluded that the molecules are not only tilted but also twisted to some extent, which can result in a slight correction of the exact angle values (see SI for details). Finally, note that the derived average tilt angle values are close to that reported for NHC SAM with ethylene side groups (30° ± 6°), also prepared by immersion procedure [8].

Thermal stability analysis

Temperature-programmed secondary ion mass spectrometry (TP-SIMS) [54] was used to probe thermal stability of the NHC SAMs in this study. Surface coverage was monitored as a function of temperature using the signal of M_2Au^+ molecular ions as a fingerprint parameter. The results of these experiments are summarized in Fig. 4, with well-defined step-like behavior for all four SAMs (Fig. 4a and d). To enable identification of the desorption temperature (T_D), derivative of the M_2Au^+ signal was calculated (Fig. 4b and e), and the corresponding peaks were fitted by the Gauss function. According to the derived values, the NHC SAMs can be separated into two groups: BIM^{iPr}/Au and IM^{Me}/Au with a T_D of ~455 K and BIM^{Me}/Au and NIM^{Me}/Au with a much higher T_D of ~620 K (as indicated by vertical dashed lines in Fig. 4). As known, desorption temperature measured in a particular experiment depends on the applied heating rate, and therefore, our T_D values cannot be directly compared with the results of former temperature-programmed desorption (TPD) experiments for NHC [11,22] and thiolate [55,56] SAMs on Au. This comparison is, however, possible in terms of the desorption energy (E_D), which can be calculated using the Redhead formula (assuming a typical value of 10^{13} Hz for the preexponential factor as also used in former analysis) [11,22,55]. The corresponding E_D values are ~1.4 eV for BIM^{iPr}/Au and IM^{Me}/Au and ~1.9 eV for BIM^{Me}/Au and NIM^{Me}/Au (Table 1). These values imply that thermal stability of the NHC SAMs dramatically depends on the molecular design and, surprisingly, the commonly applied BIM^{iPr}/Au system exhibits desorption energy which is similar to the values for thiolate SAMs on Au (E_D ~1.2–1.4 eV), obtained in the former TPD [55] and TP-SIMS [37,54,57] experiments and evaluated in the same way, with the same pre-exponential factor (10^{13} Hz). Comparison of the E_D values for BIM^{Me}/Au and BIM^{iPr}/Au shows that this parameter increases drastically (by ~0.5 eV) at the shortening of the side groups for the same molecular backbone. However, this is not the only structural parameter responsible for ultra-high thermal stability of NHC SAMs. The data obtained for IM^{Me}/Au demonstrate that despite the short side groups applied in this system, the characteristic E_D has similar, low value as for BIM^{iPr}/Au. Consequently, it is a combination of short side groups, enabling a high packing density, and an extended molecular backbone, promoting stronger intermolecular interaction and thus specific molecular organization at the molecule-metal interface, which makes BIM^{Me}/Au and NIM^{Me}/Au exceptionally stable. Whereas the fingerprint spectroscopic features of BIM^{Me}/Au, NIM^{Me}/Au and BIM^{iPr}/Au, such as the shift of the N 1s peak in XPS (Fig. 2c) and the splitting of the π* resonance in N K-edge NEXAFS (Fig. S17), manifest different molecular organization and, probably, different bonding configuration than in IM^{Me}/Au, the low packing density of BIM^{iPr}/Au renders this system only moderately stable.

The low (BIM^{iPr}/Au and IM^{Me}/Au) or high (BIM^{Me}/Au and NIM^{Me}/Au) thermal stability of NHC SAMs correlate with the specific character

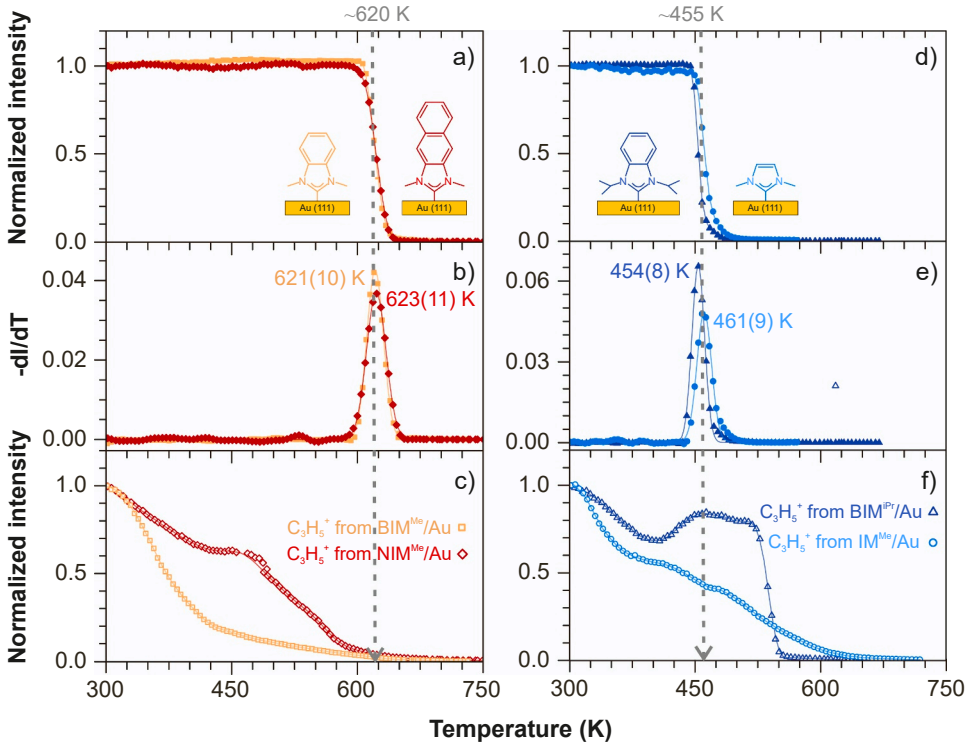

Fig. 4. Thermal stability analysis by TP-SIMS. (a,d) Normalized M_2Au^+ signal (M - complete NHC molecule) as a function of temperature for BIM^{Me}/ NIM^{Me} (a) and IM^{Me}/ BIM^{iPr} (d) SAMs on Au. Solid lines represent spline function fitted to the data. (b,e) Derivatives (dI/dT) of the data shown in (a) and (d), respectively, with the indicated T_D values determined by fitting the respective peaks with Gauss function (solid line). The accuracy of T_D is given by standard deviation. (c,f) Normalized $C_3H_5^+$ signal as a function of temperature for BIM^{Me}/ NIM^{Me} (c) and IM^{Me}/ BIM^{iPr} (f) SAMs on Au.

of the desorption process in these systems. As a representative marker in this context, the emission of $C_3H_5^+$ ions ($m/z = 41$), was monitored. The intensity of the respective signal is presented as a function of temperature in Fig. 4c and f. Importantly, the emission of $C_3H_5^+$ ions from the NHC SAMs exhibiting low thermal stability (IM^{Me}/Au and BIM^{iPr}/Au) occurs not only below but also well above the drop in the M_2Au^+ signal at $T_D \sim 455$ K. This means that the desorption process in these monolayers does not necessarily proceed via desorption of complete molecules but involves molecular fragmentation, with the subsequent emission of smaller fragments, such as $C_3H_5^+$, at higher temperatures. In contrast, for the NHC SAMs with high thermal stability (BIM^{Me}/Au and NIM^{Me}/Au), $C_3H_5^+$ emission is not perceptible for temperatures higher than the drop in the M_2Au^+ signal at $T_D \sim 620$ K, suggesting molecular desorption as the predominant temperature-induced process. Interestingly, the pronounced $C_3H_5^+$ desorption peak for BIM^{iPr}/Au at $T_D \sim 537$ K (Fig. S21) corresponds to $E_D \sim 1.64$ eV which exactly matches the desorption energy reported in the previous TPD study for BIM^{iPr}/Au, where corresponding analysis was not conducted by monitoring the emission of the complete molecular ions but by using $C_3H_5^+$ or even smaller fragments [11,22]. This difference in analytical approach can, therefore, explain the significantly higher value of desorption energy ($E_D \sim 1.64$ eV) reported earlier [11] for BIM^{iPr}/Au, compared to the current experiments ($E_D \sim 1.40$ eV). We also note that for all NHC SAMs the emission of the $C_3H_5^+$ is visible also at temperatures below the characteristic desorption temperature of the monolayer. However, with the exception of BIM^{iPr}/Au, the $C_3H_5^+$ signal does not increase or remain constant but decreases progressively in this temperature range, with constant level of the M_2Au^+ emission at the same time. Such behaviour is characteristic of desorption of a contamination rather than molecular decomposition. The respective advantageous hydrocarbons could be adsorbed on the samples during the given *ex situ* preparation, considering in particular the hydrophilic character of the NHC SAMs, as documented by the surface energy values presented in Tables 1 and S2. Small contamination does not affect the film thickness significantly, but can be readily detected by an extremely sensitive technique such as SIMS.

Conclusions

In summary, in-depth analysis of the film thickness, packing density, and molecular inclination in custom-designed series of model NHC SAMs on Au(111) unequivocally demonstrates that, contrary to the well-established opinion [14,22,23,26,27], application of short methyl side groups attached to the nitrogen heteroatoms of imidazolium allows for fabrication of upright-oriented monolayers without formation of flat-lying NHC-Au-NHC complexes. We stress at this point that in all former studies [22,23,26,27], in which laying-down orientation of NHCs with methyl side groups on Au was reported, the analyzed monolayers were deposited under vacuum conditions, in contrast to solution-based approach used in the current experiments. The application of this procedure to the NHCs with methyl side groups allowed to roughly double the packing density of NHC molecules on Au, rendering it close to the densities of the archetypical thiolate SAMs. We note at this point that the structural differences for NHC SAMs prepared by vacuum and solution based deposition were also reported before on Pt(111) surface but indicated, contrary to our data, a lower packing density (not quantified) for the liquid phase preparation [25]. However, besides using different, and much more reactive, Pt(111) substrate, the former study [25] was conducted for NHC SAMs with the large 2,4-dinitrobenzole side groups in contrast to short methyl side groups analyzed in the current experiments. This comparison with the former study confirms a well-known fact that formation of SAMs structure is a result of rather fragile balance of different competing interactions [1,2]. In comparison to vacuum deposition the presence of solvents adds even more complexity to the system via interactions of solvent molecules with the solute and the substrate, which can affect the flux of NHC molecules towards the surface, as well as their adsorption and desorption rates during monolayer formation leading to modification of the final SAM structure. Recent progress in molecular dynamic (MD) simulations of SAMs formation, which includes also solvent molecules [58], may shed some light on the exact mechanism connecting adsorption geometry of NHC SAMs with the presence of solvent. Such MD studies are beyond the scope of current work but the results reported here will hopefully stimulate dedicated research by others.

The most striking result of the current optimization of NHC SAMs is their thermal stability. Our experiments demonstrate that the reduced size of the side groups (from bulky isopropyl to small methyl) in combination with the extension of the molecular backbone (from imidazolium to benzoimidazolium or naphthaleneimidazolium) result in dramatic improvement in thermal stability of NHC SAMs, emphasized by 165 K increase in the desorption temperature (at the given heating rate), ~0.5 eV increase in the desorption energy, and the lack of molecular fragmentation.

Altogether, the obtained results provide well-defined concept of molecular design and the preparation procedure, paving the way to the fabrication of densely packed and thermally ultra-stable functional aromatic SAMs on the NHC basis. Such SAMs can be particularly useful for applications in organic and molecular electronics where the high thermal stability of functional monolayers becomes frequently critical considering (i) thermal processing steps during the assembly of a particular device [5] and (ii) overheating problems related to a poor heat transport at the molecule-metal interface due to the mismatch between the vibrational density of states of the organic and inorganic parts of the molecule-metal junction [59]. Whereas non-substituted molecules were used in the present basic study, different substitutions can be introduced, making, at the given packing density and upright molecular orientation, a desired chemical and physical impact for a particular surface or interface. The suggested solution-based preparation procedure simplifies the assembly of devices, making the use of NHC SAMs attractive also in this regard.

Declaration of Competing Interest

The authors declare that they have no known competing financial interests or personal relationships that could have appeared to influence the work reported in this paper.

Data availability

Data will be made available on request.

Acknowledgments

The authors would like to thank Marek Drozdek (Faculty of Chemistry, Jagiellonian University) and Paweł Dąbczyński (Institute of Physics, Jagiellonian University) for their assistance in collecting XPS and SIMS data, respectively. Allocation of synchrotron radiation beamtimes at BESSY II (Helmholtz Zentrum Berlin) is highly appreciated. This work was supported financially by the National Science Centre Poland (grant DEC-2018/31/B/ST5/00057). The HRMS equipment was supported by a grant from the Faculty of Chemistry under the Strategic Programme Excellence Initiative at Jagiellonian University. A. A. acknowledges the financial support by the DAAD-ACEH Scholarship of Excellence.

Appendix A. Supporting information

Supplementary data associated with this article can be found in the online version at doi:10.1016/j.nantod.2023.102024.

References

[1] J.C. Love, L.A. Estroff, J.K. Kriebel, R.G. Nuzzo, G.M. Whitesides, Self-assembled monolayers of thiolates on metals as a form of nanotechnology, Chem. Rev. 105 (2005) 1103–1170, https://doi.org/10.1021/cr0300789.

[2] J.J. Gooding, S. Ciampi, The molecular level modification of surfaces: from self-assembled monolayers to complex molecular assemblies, Chem. Soc. Rev. 40 (2011) 2704–2718, https://doi.org/10.1039/c0cs00139b.

[3] Y. Dai, C.C. Liu, Recent advances on electrochemical biosensing strategies toward universal point-of-care systems, Angew. Chem. Int. Ed. 58 (2019) 12355–12368, https://doi.org/10.1002/anie.201901879.

[4] H. Cui, W. Wang, L. Shi, W. Song, S. Wang, Superwettable surface engineering in controlling cell adhesion for emerging bioapplications, Small Methods 4 (2020), https://doi.org/10.1002/smtd.202000573.

[5] A. Vilan, D. Aswal, D. Cahen, Large-area, ensemble molecular electronics: motivation and challenges, Chem. Rev. 117 (2017) 4248–4286, https://doi.org/10.1021/acs.chemrev.6b00595.

[6] R.M. Metzger, Unimolecular electronics, Chem. Rev. 115 (2015) 5056–5115, https://doi.org/10.1021/cr500459d.

[7] H. Häkkinen, The gold-sulfur interface at the nanoscale, Nat. Chem. 4 (2012) 443–455, https://doi.org/10.1038/nchem.1352.

[8] T. Weidner, J.E. Baio, A. Mundstock, C. Große, S. Karthäuser, C. Bruhn, U. Siemeling, NHC-based self-assembled monolayers on solid gold substrates, Aust. J. Chem. 64 (2011) 1177–1179, https://doi.org/10.1071/CH11173.

[9] A. v Zhukhovitskiy, M.G. Mavros, T. van Voorhis, J.A. Johnson, Addressable carbene anchors for gold surfaces, J. Am. Chem. Soc. 135 (2013) 7418–7421, https://doi.org/10.1021/ja401965d.

[10] C.M. Crudden, J.H. Horton, I.I. Ebralidze, O. v Zenkina, A.B. McLean, B. Drevniok, Z. She, H.B. Kraatz, N.J. Mosey, T. Seki, E.C. Keske, J.D. Leake, A. Rousina-Webb, G. Wu, Ultra stable self-assembled monolayers of N-heterocyclic carbenes on gold, Nat. Chem. 6 (2014) 409–414, https://doi.org/10.1038/nchem.1891.

[11] C.M. Crudden, J.H. Horton, M.R. Narouz, Z. Li, C.A. Smith, K. Munro, C. J. Baddeley, C.R. Larrea, B. Drevniok, B. Thanabalasingam, A.B. McLean, O. v Zenkina, I.I. Ebralidze, Z. She, H.B. Kraatz, N.J. Mosey, L.N. Saunders, A. Yagi, Simple direct formation of self-assembled N-heterocyclic carbene monolayers on gold and their application in biosensing, Nat. Commun. 7 (2016), https://doi.org/10.1038/ncomms12654.

[12] S. Park, S. Kang, H.J. Yoon, Thermopower of molecular junction in harsh thermal environments, Nano Lett. 22 (2022) 3953–3960, https://doi.org/10.1021/acs.nanolett.2c00422.

[13] C. Deng, J. Chen, Q. Tang, Theoretical investigation on the adsorption and interface bonding between N-heterocyclic carbenes and metal surfaces, J. Phys. Chem. C 125 (2021) 4489–4497, https://doi.org/10.1021/acs.jpcc.0c09899.

[14] M. Jain, U. Gerstmann, W.G. Schmidt, H. Aldahhak, Adatom mediated adsorption of N-heterocyclic carbenes on Cu(111) and Au(111), J. Comput. Chem. 43 (2022) 413–420, https://doi.org/10.1002/jcc.26801.

[15] A. Asyuda, S. Das, M. Zharnikov, Thermal stability of alkanethiolate and aromatic thiolate self-assembled monolayers on Au(111): an X-ray photoelectron spectroscopy study, J. Phys. Chem. C 125 (2021) 21754–21763, https://doi.org/10.1021/acs.jpcc.1c06984.

[16] E. Amit, I. Berg, E. Gross, Self-assembled monolayers of nitron: self-activated and chemically addressable N-heterocyclic carbene monolayers with triazolone structural motif, Chem. Eur. J. 26 (2020) 13046–13052, https://doi.org/10.1002/chem.202001595.

[17] A. Bakker, M. Freitag, E. Kolodzeiski, P. Bellotti, A. Timmer, J. Ren, B. Schulze Lammers, D. Moock, H.W. Roesky, H. Mönig, S. Amirjalayer, H. Fuchs, F. Glorius, An electron-rich cyclic (alkyl)(amino)carbene on Au(111), Ag(111), and Cu(111) surfaces, Angew. Chem. Int. Ed. 59 (2020) 13643–13646, https://doi.org/10.1002/anie.201915618.

[18] L.M. Sherman, S.L. Strausser, R.K. Borsari, D.M. Jenkins, J.P. Camden, Imidazolinium N-heterocyclic carbene ligands for enhanced stability on gold surfaces, Langmuir 37 (2021) 5864–5871, https://doi.org/10.1021/acs.langmuir.1c00314.

[19] C.A. Smith, M.R. Narouz, P.A. Lummis, I. Singh, A. Nazemi, C.H. Li, C.M. Crudden, N-heterocyclic carbenes in materials chemistry, Chem. Rev. 119 (2019) 4986–5056, https://doi.org/10.1021/acs.chemrev.8b00514.

[20] S. Engel, E.C. Fritz, B.J. Ravoo, New trends in the functionalization of metallic gold: from organosulfur ligands to N-heterocyclic carbenes, Chem. Soc. Rev. 46 (2017) 2057–2075, https://doi.org/10.1039/c7cs00023e.

[21] M. Koy, P. Bellotti, M. Das, F. Glorius, N-heterocyclic carbenes as tunable ligands for catalytic metal surfaces, Nat. Catal. 4 (2021) 352–363, https://doi.org/10.1038/s41929-021-00607-z.

[22] C.R. Larrea, C.J. Baddeley, M.R. Narouz, N.J. Mosey, J.H. Horton, C.M. Crudden, N-heterocyclic carbene self-assembled monolayers on copper and gold: dramatic effect of wingtip groups on binding, orientation and assembly, ChemPhysChem 18 (2017) 3536–3539, https://doi.org/10.1002/cphc.201701045.

[23] L. Jiang, B. Zhang, G. Médard, A.P. Seitsonen, F. Haag, F. Allegretti, J. Reichert, B. Kuster, J.v. Barth, A.C. Papageorgiou, N-heterocyclic carbenes on close-packed coinage metal surfaces: Bis-carbene metal adatom bonding scheme of monolayer films on Au, Ag and Cu, Chem. Sci. 8 (2017) 8301–8308, https://doi.org/10.1039/c7sc03777e.

[24] S. Dery, P. Bellotti, T. Ben-Tzvi, M. Freitag, T. Shahar, A. Cossaro, A. Verdini, L. Floreano, F. Glorius, E. Gross, Influence of N-substituents on the adsorption geometry of OH-functionalized chiral N-heterocyclic carbenes, Langmuir 37 (2021) 10029–10035, https://doi.org/10.1021/acs.langmuir.1c01199.

[25] S. Dery, S. Kim, G. Tomaschun, I. Berg, D. Feferman, A. Cossaro, A. Verdini, L. Floreano, T. Klüner, F.D. Toste, E. Gross, Elucidating the influence of anchoring geometry on the reactivity of no2-functionalized n-heterocyclic carbene monolayers, J. Phys. Chem. Lett. 10 (2019) 5099–5104, https://doi.org/10.1021/acs.jpclett.9b01808.

[26] A. Inayeh, R.R.K. Groome, I. Singh, A.J. Veinot, F.C. de Lima, R.H. Miwa, C. M. Crudden, A.B. McLean, Self-assembly of N-heterocyclic carbenes on Au(111, Nat. Commun. 12 (2021), https://doi.org/10.1038/s41467-021-23940-0.

[27] G. Lovat, E.A. Doud, D. Lu, G. Kladnik, M.S. Inkpen, M.L. Steigerwald, D. Cvetko, M.S. Hybertsen, A. Morgante, X. Roy, L. Venkataraman, Determination of the structure and geometry of N-heterocyclic carbenes on Au(111) using high-resolution spectroscopy, Chem. Sci. 10 (2019) 930–935, https://doi.org/10.1039/c8sc03502d.

[28] S. Dery, S. Kim, G. Tomaschun, D. Haddad, A. Cossaro, A. Verdini, L. Floreano, T. Klüner, F.D. Toste, E. Gross, Flexible NO2-functionalized N-heterocyclic carbene monolayers on Au (111) surface, Chem. Eur. J. (2019), https://doi.org/10.1002/chem.201903434.

[29] Q. Tang, D.E. Jiang, Comprehensive view of the ligand-gold interface from first principles, Chem. Mater. 29 (2017) 6908–6915, https://doi.org/10.1021/acs.chemmater.7b02297.

[30] G. Wang, A. Rühling, S. Amirjalayer, M. Knor, J.B. Ernst, C. Richter, H.J. Gao, A. Timmer, H.Y. Gao, N.L. Doltsinis, F. Glorius, H. Fuchs, Ballbot-type motion of N-heterocyclic carbenes on gold surfaces, Nat. Chem. 9 (2017) 152–156, https://doi.org/10.1038/NCHEM.2622.

[31] A. Bakker, A. Timmer, E. Kolodzeiski, M. Freitag, H.Y. Gao, H. Mönig, S. Amirjalayer, F. Glorius, H. Fuchs, Elucidating the binding modes of N-heterocyclic carbenes on a gold surface, J. Am. Chem. Soc. 140 (2018) 11889–11892, https://doi.org/10.1021/jacs.8b06180.

[32] E. Angove, F. Grillo, H.A. Früchtl, A.J. Veinot, I. Singh, J.H. Horton, C.M. Crudden, C.J. Baddeley, Highly ordered N-heterocyclic carbene monolayers on Cu(111), J. Phys. Chem. Lett. 13 (2022) 2051–2056, https://doi.org/10.1021/acs.jpclett.1c04073.

[33] A.J. Veinot, A. Al-Rashed, J.D. Padmos, I. Singh, D.S. Lee, M.R. Narouz, P. A. Lummis, C.J. Baddeley, C.M. Crudden, J.H. Horton, N-heterocyclic carbenes reduce and functionalize copper oxide surfaces in one pot, Chem. Eur. J. 26 (2020) 11431–11434, https://doi.org/10.1002/chem.202002308.

[34] M.R. Narouz, K.M. Osten, P.J. Unsworth, R.W.Y. Man, K. Salorinne, S. Takano, R. Tomihara, S. Kaappa, S. Malola, C.T. Dinh, J.D. Padmos, K. Ayoo, P.J. Garrett, M. Nambo, J.H. Horton, E.H. Sargent, H. Häkkinen, T. Tsukuda, C.M. Crudden, N-heterocyclic carbene-functionalized magic-number gold nanoclusters, Nat. Chem. 11 (2019) 419–425, https://doi.org/10.1038/s41557-019-0246-5.

[35] M.J. MacLeod, A.J. Goodman, H.Z. Ye, H.V.T. Nguyen, T. van Voorhis, J. A. Johnson, Robust gold nanorods stabilized by bidentate N-heterocyclic-carbene–thiolate ligands, Nat. Chem. 11 (2019) 57–63, https://doi.org/10.1038/s41557-018-0159-8.

[36] B. Arezki, A. Delcorte, B.J. Garrison, P. Bertrand, Understanding gold-thiolate cluster emission from self-assembled monolayers upon kiloelectronvolt ion bombardment, J. Phys. Chem. B 110 (2006) 6832–6840, https://doi.org/10.1021/jp058252f.

[37] A. Krzykawska, M. Wróbel, K. Kozieł, P. Cyganik, N-heterocyclic carbenes for the self-assembly of thin and highly insulating monolayers with high quality and stability, ACS Nano 14 (2020) 6043–6057, https://doi.org/10.1021/acsnano.0c01733.

[38] M. Rodríguez-Castillo, G. Lugo-Preciado, D. Laurencin, F. Tielens, A. van der Lee, S. Clément, Y. Guari, J.M. López-de-Luzuriaga, M. Monge, F. Remacle, S. Richeter, Experimental and theoretical study of the reactivity of gold nanoparticles towards benzimidazole-2-ylidene ligands, Chem. Eur. J. 22 (2016) 10446–10458, https://doi.org/10.1002/chem.201601253.

[39] K. Chang, J.G. Chen, Q. Lu, M.J. Cheng, Quantum mechanical study of N-heterocyclic carbene adsorption on Au surfaces, J. Phys. Chem. A 121 (2017) 2674–2682, https://doi.org/10.1021/acs.jpca.7b01153.

[40] D. Nolting, N. Ottosson, M. Faubel, I.v. Hertel, B. Winter, Pseudoequivalent nitrogen atoms in aqueous imidazole distinguished by chemical shifts in photoelectron spectroscopy, J. Am. Chem. Soc. 130 (2008) 8150–8151, https://doi.org/10.1021/ja8022384.

[41] J. Ossowski, T. Wächter, L. Silies, M. Kind, A. Noworolska, F. Blobner, D. Gnatek, J. Rysz, M. Bolte, P. Feulner, A. Terfort, P. Cyganik, M. Zharnikov, Thiolate versus selenolate: structure, stability, and charge transfer properties, ACS Nano 9 (2015) 4508–4526, https://doi.org/10.1021/acsnano.5b01109.

[42] T. Weidner, A. Shaporenko, J. Müller, M. Schmid, P. Cyganik, A. Terfort, M. Zharnikov, Effect of the bending potential on molecular arrangement in alkaneselenolate self-assembled monolayers, J. Phys. Chem. C 112 (2008) 12495–12506, https://doi.org/10.1021/jp8044077.

[43] T.C. Taucher, I. Hehn, O.T. Hofmann, M. Zharnikov, E. Zojer, Understanding chemical versus electrostatic shifts in X-ray photoelectron spectra of organic self-assembled monolayers, J. Phys. Chem. C 120 (2016) 3428–3437, https://doi.org/10.1021/acs.jpcc.5b12387.

[44] S. Fischer, A.C. Papageorgiou, M. Marschall, J. Reichert, K. Diller, F. Klappenberger, F. Allegretti, A. Nefedov, C. Wöll, J.v. Barth, L-Cysteine on Ag (111): a combined STM and X-ray spectroscopy study of anchorage and deprotonation, J. Phys. Chem. C 116 (2012) 20356–20362, https://doi.org/10.1021/jp305270h.

[45] O. Dannenberger, K. Weiss, H. Himmel, M. Buck, An orientation analysis of differently endgroup-functionalised alkanethiols adsorbed on Au substrates, Thin Solid Films 307 (1997) 183–191, https://doi.org/10.1016/S0040-6090(97)00280-0.

[46] C.L.A. Lamont, J. Wilkes, Attenuation length of electrons in self-assembled monolayers of n-alkanethiols on gold, Langmuir 15 (1999) 2037–2042, https://doi.org/10.1021/la981168p.
[47] D. Gnatek, S. Schuster, J. Ossowski, M. Khan, J. Rysz, S. Krakert, A. Terfort, M. Zharnikov, P. Cyganik, Odd-even effects in the structure and stability of azobenzene-substituted alkanethiolates on Au(111) and Ag(111) substrates, J. Phys. Chem. C 119 (2015) 25929–25944, https://doi.org/10.1021/acs.jpcc.5b07899.
[48] E. Apen, A.P. Hitchcock, J.L. Gland, Experimental studies of the core excitation of imidazole, 4,5-dicyanoimidazole, and s-triazine, J. Phys. Chem. 97 (1993) 6859–6866, https://doi.org/10.1021/j100128a019.
[49] F. Meyer, M. Blum, A. Benkert, D. Hauschild, Y.L. Jeyachandran, R.G. Wilks, W. Yang, M. Bär, F. Reinert, C. Heske, M. Zharnikov, L. Weinhardt, Site-specific electronic structure of imidazole and imidazolium in aqueous solutions, Phys. Chem. Chem. Phys. 20 (2018) 8302–8310, https://doi.org/10.1039/c7cp07885d.
[50] J.F. Walsh, H.S. Dhariwal, A. Gutiérrez-Sosa, P. Finetti, C.A. Muryn, N.B. Brookes, R.J. Oldman, G. Thornton, Probing molecular orientation in corrosion inhibition via a NEXAFS study of benzotriazole and related molecules on Cu(100), Surf. Sci. 415 (1998) 423–432, https://doi.org/10.1016/S0039-6028(98)00604-9.
[51] S. Dery, S. Kim, D. Haddad, A. Cossaro, A. Verdini, L. Floreano, F.D. Toste, E. Gross, Identifying site-dependent reactivity in oxidation reactions on single Pt particles, Chem. Sci. 9 (2018) 6523–6531, https://doi.org/10.1039/c8sc01956h.
[52] S. Dery, I. Berg, S. Kim, A. Cossaro, A. Verdini, L. Floreano, F.D. Toste, E. Gross, Strong metal-adsorbate interactions increase the reactivity and decrease the orientational order of OH-functionalized N-heterocyclic carbene monolayers, Langmuir 36 (2020) 697–703, https://doi.org/10.1021/acs.langmuir.9b02401.
[53] F. Crasto De Lima, A. Fazzio, A.B. McLean, R.H. Miwa, Simulations of X-ray absorption spectroscopy and energetic conformation of N-heterocyclic carbenes on Au(111), Phys. Chem. Chem. Phys. 22 (2020) 21504–21511, https://doi.org/10.1039/d0cp04240d.
[54] D. Rading, R. Kersting, A. Benninghoven, Secondary ion emission from molecular overlayers: thiols on gold, J. Vac. Sci. Technol. A 18 (2000) 312–319, https://doi.org/10.1116/1.582185.
[55] D.J. Lavrich, S.M. Wetterer, S.L. Bernasek, G. Scoles, Physisorption and chemisorption of alkanethiols and alkyl sulfides on Au(111), J. Phys. Chem. B 102 (1998) 3456–3465, https://doi.org/10.1021/jp980047v.
[56] E. Ito, H. Ito, H. Kang, T. Hayashi, M. Hara, J. Noh, Influence of surface morphology and substrate on thermal stability and desorption behavior of octanethiol self-assembled monolayers: Cu, Ag, and Au, J. Phys. Chem. C 116 (2012) 17586–17593, https://doi.org/10.1021/jp3041204.
[57] J. Ossowski, G. Nascimbeni, T. Zaba, E. Verwüster, J. Rysz, A. Terfort, M. Zharnikov, E. Zojer, P. Cyganik, Relative thermal stability of thiolate- and selenolate-bonded aromatic monolayers on the Au(111) substrate, J. Phys. Chem. C 121 (2017) 28031–28042, https://doi.org/10.1021/acs.jpcc.7b09685.
[58] P. Bhadra, S.W.I. Siu, Effect of concentration, chain length, hydrophobicity, and an external electric field on the growth of mixed alkanethiol self-assembled monolayers: a molecular dynamics study, Langmuir 37 (2021) 1913–1924, https://doi.org/10.1021/acs.langmuir.0c03414.
[59] M.D. Losego, M.E. Grady, N.R. Sottos, D.G. Cahill, P.V. Braun, Effects of chemical bonding on heat transport across interfaces, Nat. Mater. 11 (2012) 502–506, https://doi.org/10.1038/nmat3303.